ACS APPLIED MATERIALS & INTERFACES

Research Article

www.acsami.org

Enhancing Photocatalytic Activity of Graphitic Carbon Nitride by Codoping with P and C for Efficient Hydrogen Generation

Hao Wang,[†] Bo Wang,[†] Yaru Bian,[†] and Liming Dai*[,†,‡]

[†]BUCT-CWRU International Joint Laboratory, State Key Laboratory of Organic−Inorganic Composites, Center for Soft Matter Science and Engineering, College of Energy, Beijing University of Chemical Technology, Beijing, China

[‡]Center of Advanced Science and Engineering for Carbon (Case4Carbon), Department of Macromolecular Science and Engineering, Case Western Reserve University, 10900 Euclid Avenue, Cleveland, Ohio 44106, United States

Supporting Information

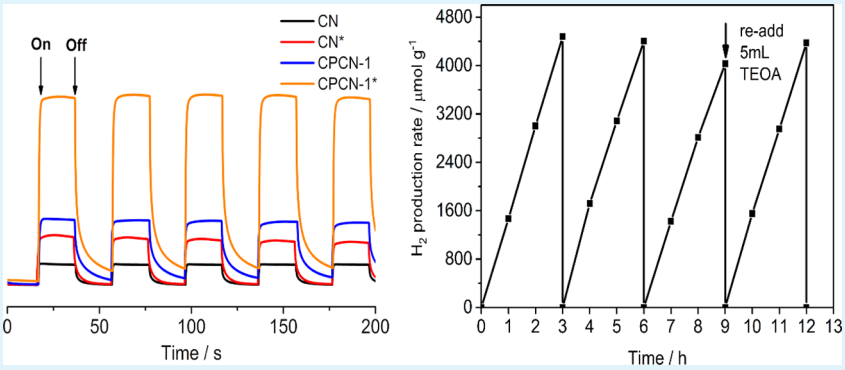

ABSTRACT: The generation of clean hydrogen gas from photocatalytic water splitting by using graphitic carbon nitride (g-C_3N_4) as the photocatalyst has attracted considerable research interest. For practical applications, however, the photocatalytic activity of g-C_3N_4 needs to be further improved by, for example, band gap engineering through heteroatom doping. In this study, we found that doping of carbon nitride with carbon and phosphorus (P) could tune energy level of the conduction band. Subsequent hydrothermal treatment led to an increase in the specific surface area from 24.9 up to 141.1 m^2 g^{-1}, which was accompanied by increasing C concentration of the resultant C, P-doped g-C_3N_4 to reduce the hole−electron recombination and enhance the conductivity. Consequently, the C, P-codoped g-C_3N_4 (i.e., CPCN-1*) exhibited a much enhanced photocatalytic activity for efficient generation of H_2 by photocatalytic water splitting under visible-light irradiation (1493.3 μmol g^{-1} h^{-1}—about 9.7 times enhancement from that of bulk g-C_3N_4).

KEYWORDS: *graphitic carbon nitride, doping, band gap, pore structure, hydrogen generation*

1. INTRODUCTION

Clean hydrogen generation by splitting water with sunlight plays an important role in developing sustainable green energy.[1−4] As first reported by Antonietti and co-workers, graphitic carbon nitride (g-C_3N_4) having an intrinsic band gap of ∼2.7 eV could be used as a catalyst for photogeneration of hydrogen from water with visible light irradiation.[5] Since then, g-C_3N_4 has been widely studied for photocatalytic water splitting and many other reactions, such as oxygen reduction, water treatment, and organic pollutants degradation.[4,6−11] Furthermore, g-C_3N_4 was found to be chemically/thermally stable and nontoxic, providing additional advantages for photocatalysis and/or photodynamic therapy.[2,5,12,13] However, photocatalytic performance of the pristine g-C_3N_4 is still suffered from multidisadvantages, including its low electrical conductivity, narrow adsorption range of visible light, high recombination rate of carriers, and ease with which g-C_3N_4 aggregates in the conventional fabrication process.[14−17] To overcome these deficiencies, a few approaches involving the control of morphology, modulation of electronic structure by heteroatom doping, and creation of heterojunctions with other semiconductors have been reported recently.[2,6,18−21] Among them, the heteroatom-doping approach is of particular interest as it could simultaneously tune energy levels of the valence band (VB), conduction band (CB), visible light absorption efficiency, and charge transfer mobility.[2,22−27] Indeed, doping of g-C_3N_4 with B, P, N, S, and/or F has been demonstrated to efficiently improve its photocatalytic activity.[23,28−30] Nevertheless, possible effects of codoping on the photocatalytic activity of g-C_3N_4 have been much less discussed in the literature. Besides, it is important to enlarge the specific surface areas (SSA) of a photocatalyst.[31−37]

In this study, we developed a facile but efficient synthetic route to prepare C, P-codoped g-C_3N_4 by self-assembling

Received: February 19, 2017
Accepted: May 30, 2017
Published: May 30, 2017

DOI: 10.1021/acsami.7b02445
ACS Appl. Mater. Interfaces 2017, 9, 21730−21737

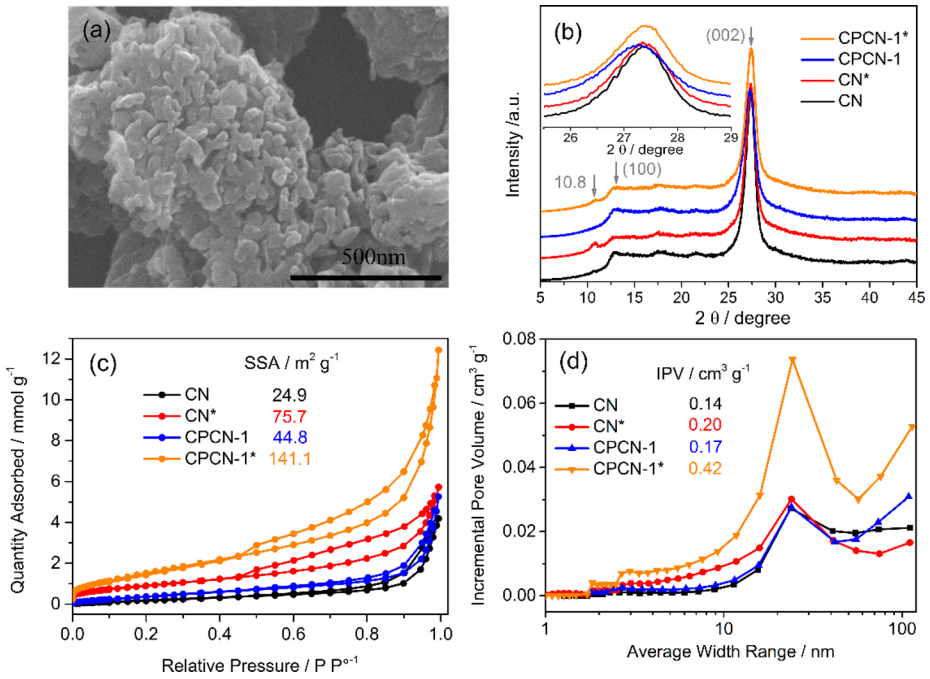

Figure 1. (a) A typical SEM image of CPCN-1*. (b) XRD patterns of CN, CN*, CPCN-1, and CPCN-1* with the inset displaying an enlarged view of the (002) peaks. (c) N_2 adsorption and desorption isotherms and (d) the corresponding pore size distributions for CN, CN*, CPCN-1, and CPCN-1*.

melamine with phytic acid,[20,38] followed by hydrothermal treatment to enlarge its specific surface area. Doping carbon species into the lattice of g-C_3N_4 has been found to reduce the hole−electron recombination by improving conductivity, which could lead to a further enhanced photocatalytic performance for hydrogen generation.[39] Compared to the pristine g-C_3N_4, our newly developed C, P-codoped g-C_3N_4 exhibited an about 9.7 times higher H_2 generation rate (1493.3 μmol g^{-1} h^{-1}) from photocatalytic water splitting under visible light, which is among the best for carbon-based metal-free photocatalysts ever reported (cf. Table S1), with a reasonably high apparent quantum efficiency (AQE) 2.14%.

2. EXPERIMENTAL SECTION

2.1. Materials Preparation. In a typical experiment, 1.0 g of melamine was dissolved into 100.0 mL of distilled water at 60 °C to obtain a homogeneous suspension, to which a predetermined amount of phytic acid (10.0 wt % in water) was then added, that is, the molarity 1.52 mol L^{-1}. Continued stirring of the mixture solution at 60 °C for 6 h led to water evaporation to produce the solid product, which was then heated up to 550 °C at a heating rate of 5 °C min^{-1} and annealed for 4 h in a tubular furnace. After being cooled down to room temperature, we collected the brown agglomerate sample and milled it into powder in a mortar for subsequent use. Samples with different C, P-doping levels were synthesized under the same conditions, but with different ratios of phytic acid to melamine in the reactants, and designated as CPCN-*X* with *X* being the molar percentage of phytic acid in the starting material. For the hydrothermal post-treatment, 150.0 mg of the resultant P-doped g-C_3N_4 was mixed with 40.0 mL of distilled water in a 50.0 mL packed Teflon-lined autoclave and heated at 180 °C for 6 h. After the hydrothermal treatment, C, P-codoped g-C_3N_4 was obtained as the final product and designated as CPCN-*X**. As reference, pristine g-C_3N_4 was also synthesized by the same procedure, but without the addition of phytic acid, and designated as CN. The pristine g-C_3N_4 after hydrothermally treated was designated as CN*.

2.2. Physicochemical Characterization. X-ray powder diffraction (XRD) was measured using a D2 PHSDER X-ray diffractometer (Bruker Company, Germany) and Cu Kα radiation (λ = 1.540 56 Å). X-ray photoelectron spectroscopy (XPS) was performed on an ESCALAB MKII X-ray photoelectron spectrometer (VG Instruments, CA, USA) using nonmonochromatized Mg Kα X-ray source. Fourier transform infrared (FT-IR) spectroscopic measurements were carried out using KBr pellets on a Nicolet 6700 FT-IR spectrometer (Thermo scientific, USA) with DLA TGS detector. UV−vis diffuse reflectance spectra (DRS) were taken on a UV-2600 spectrophotometer (Shimadzu, Japan). Photoluminescence (PL) spectroscopy was performed using an F-700 fluorescence spectrophotometer (Hitachi, Japan) with 368 nm excitation laser. Transmission electron microscope (TEM) images were acquired on a FEI Tecnai G20 field emission electron microscope operating at an accelerating voltage of 200 kV. N_2 adsorption and desorption isotherms were collected on an ASAP 2460 N_2 adsorption apparatus (Micrometritica, USA) at 77 and 273 K, respectively. The total pore volumes were estimated from the adsorbed amount of N_2 at a relative pressure P/P_0 of 0.995.

Mott−Schottky plots were recorded on an electrochemical workstation (CHI 760E) with a standard three-electrode cell by using an indium−tin oxide glass (ITO glass) precoated with various carbon nitride samples as the working electrodes, Pt wire as the counter electrode, and Ag/AgCl reference electrode in saturated KCl. The working electrode was prepared by dispersing 30.0 mg of specific carbon nitride powder in a mixture solution of 1.0 mL of ethanol, 1.0 mL of ethylene glycol, and 20.0 μL of Nafion (5 wt %), followed by drop-casting 50.0 μL of the resulted colloidal dispersion onto a piece of 2 cm long and 2 cm wide ITO glass (4 cm^2), and the area coated with photocatalysts is 2.3 cm^2. Prior to use, the resultant electrode was dried in an oven at 120 °C for 2 h. A 300 W Xe lamp with a cut filter (λ > 420 nm) was used as the light source.

2.3. Photocatalytic H_2 Evolution Measurement. Photocatalytic performance for H_2 generation was investigated in a 215.0 mL Pyrex flask with a 300 W Xe lamp (Microsolar 300, Perfect Light) as the light source. The distance between the sample and light source was 20 cm, and the intensity of incident light was 88.0 mW cm^{-2}. Typically, 50.0 mg of specific carbon nitride (CN) sample was added to an aqueous solution (100.0 mL) of triethanolamine (TEOA, 20 vol %, as a sacrificial reagent), and then ca. 1.0 wt % Pt was deposited onto the surface of CN by *in situ* photodeposition approach using H_2PtCl_6·

DOI: 10.1021/acsami.7b02445
ACS Appl. Mater. Interfaces 2017, 9, 21730−21737

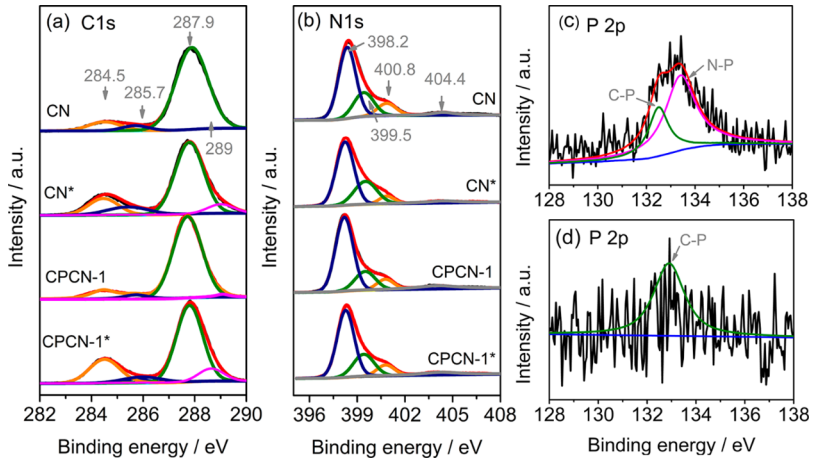

Figure 2. (a) XPS C 1s and (b) N 1s spectra of CN, CN*, CPCN-1, and CPCN-1*. XPS P 2p spectra of CPCN-1 (c) and (d) CPCN-1*.

$6H_2O$ as Pt source under a 300 W Xe lamp by irradiating for 1 h.[5] Pt was used as an "electron acceptor" to facilitate charge separation for the photoinduced carriers and subsequent electron collection. The resulting suspension was then bubbled with N_2 at flow of 200 sccm for 0.5 h to remove air. After irradiation under visible light from the 300 W Xe lamp (Microsolar300, Perfect Light with a cut filter, $\lambda > 420$ nm) for 3 h, 0.5 mL of the released gas was sampled. A gas chromatograph (TCD with N_2 as a carrier gas and 5 Å molecular sieve column, GC-2014C, SHIMADZU) was employed to test the amount of H_2 generated. The stability of photocatalyst was measured using the same protocol with a prolonged sampling duration. The apparent quantum efficiency (AQE) was measured under the same reaction condition with a band-pass filter ($\lambda = 420$ nm) and an irradiation time of 10 h. The AQE value was calculated according to eq S1, and the calculation details of H_2-generation rate and AQE are listed in the Supporting Information.

3. RESULTS AND DISCUSSION

Since our preliminary results indicated that CPCN-1 showed the highest photocatalytic H_2-generation performance among CPCN-*X* (*X* = 0.5, 0.75, 1, 1.25, 1.5) due to its proper crystallinity and dopant concentration (Figures S1 and S7), we chose CPCN-1 for the subsequent hydrothermal post-treatment to produce CPCN-1* (Supporting Information). Figure 1a reproduces a SEM image of CPCN-1*, which shows a granular morphology. The powder XRD patterns given in Figure 1b show two characteristic peaks at 13.01° and 27.41° attributable to the (100) and (002) lattice plane, respectively, for all the carbon nitride samples studied.[5,40] As can be seen in the inset of Figure 1b, the (002) peak of CPCN-1 shifted slightly to a lower degree of 27.23° from 27.41° for CN due to a small lattice expansion along the *c*-axis caused by doping with the relatively large P atoms into the carbon nitride structure. For CPCN-*X* samples with an increased amount of phytic acid (from 0.5 to 1.5 mol %) in the starting materials, the (002)/(001) peak intensity ratio gradually decreased with increasing *X* (Figure S1) in consistence with the P-doping induced lattice expansion. As noticed in Figure 1b with care, the relative intensity of the (002) peak to (100) peak for hydrothermally treated CN* and CPCN-1* is lower than that of their counterparts (i.e., CN and CPCN-1, respectively), indicating slight interplanar stacking disorders caused by the hydrothermal post-treatment. The newly appeared small peak at ~10.8° for samples after the hydrothermal post-treatment (i.e., CN*, CPCN-1*) is associated with the melem-like structure (e.g., $-NH/NH_2$) formed during the hydrothermal treatment.[41,42] As seen in the inset of Figure 1b, the (002) peak of CPCN-1 at 27.23° shifted back to a higher degree of 27.39° for CPCN-1* after the hydrothermal post-treatment due, most probably, to the thermal leaching of P atoms out of the crystalline lattice, as also confirmed by a concomitant decrease in the P content from 0.29% in CPCN-1 to 0.14% in CPCN-1* measured by XPS (*vide infra*).[26,35,39] Partical P leaching and framework decomposition could largely increase the volume of mesopores (Figure 1d) to facilitate the mass transport of electrolyte.

Fourier transform infrared (FT-IR) spectra were measured to characterize functional groups in the carbon nitride samples. As seen in Figure S2, the typical skeletal stretching vibrations of CN heterocycle appeared over 1200−1650 cm^{-1}.[43] The breathing mode of heptazine rings was also seen at 809 cm^{-1}, indicating heptazine rings as the building block.[44] The broad adsorption band over 2900 to 3500 cm^{-1} is arising from the N−H and N−H_2 stretching vibrations.[35,37] The adsorption peak centered at 3430 cm^{-1} could be attributed to the stretching vibrations of adsorbed water molecules. As shown in both SEM (Figure S5) and TEM (Figure S6) images, hydrothermal treatment reduced the particle size and made the CN* surface rougher with slightly curled edges, leading to a more porous structure useful for photocatalysis. To measure the specific surface area (i.e., Brunauer−Emmett−Teller, BET, specific surface area) and porosity, we perform the N_2 adsorption and desorption measurements. As shown in Figures 1c and 1d, C, P-doping significantly increased the specific surface area (SSA) from 24.9 $m^2\ g^{-1}$ (CN) to 44.8 $m^2\ g^{-1}$ (CPCN-1). Hydrothermal post-treatment further reduced the particle size by partial decomposition of the framework through losing N and leaching P (Figure S4) and increased the SSA from 24.9 $m^2\ g^{-1}$ for CN to 75.7 $m^2\ g^{-1}$ for CN* and from 44.8 $m^2\ g^{-1}$ for CPCN-1 to 141.1 $m^2\ g^{-1}$ for CPCN-1* (Figure 1c). The overall more than 3 times increase in the specific surface area by C, P-doping and hydrothermal post-treatment could make CPCN-1* and its analogous as efficient (photo)catalysts.

X-ray photoelectron spectroscopy was applied to study the evolution of chemical bonds and element composition changes during the materials preparation. Figure S4 shows XPS survey spectra for all samples, from which we can see the presence of C and P in CPCN-1 (Figure S3c and Table S1) and the hydrothermal further increasing C concentration in CPCN-1*, as the percentage content of C increased from about 42.04% for CPCN-1 (Figure S3c) to 46.30% for CPCN-1* (Figure S3d) while P slightly bleached (cf. inset of Figure 1b). The high-

DOI: 10.1021/acsami.7b02445
ACS Appl. Mater. Interfaces 2017, 9, 21730−21737

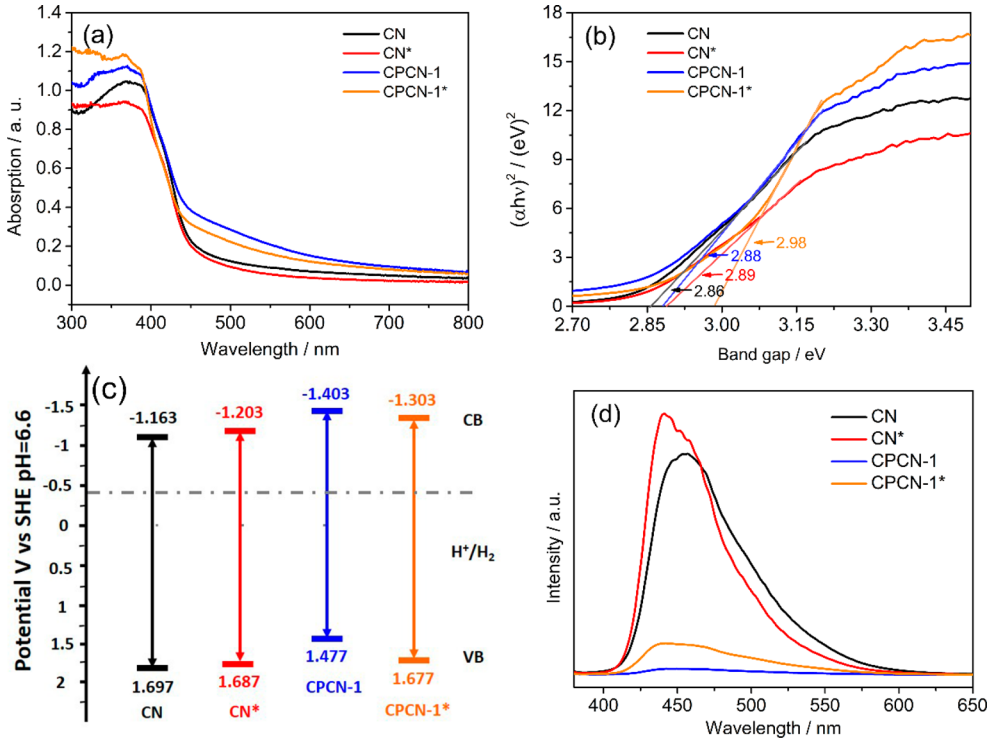

Figure 3. (a) UV−vis diffuse reflectance spectra (DRS), (b) Tauc plot, (c) electronic band gap structure in 0.2 M Na_2SO_4 aqueous solutions, and (d) PL spectra of CN, CN*, CPCN-1, and CPCN-1* with an excitation wavelength of 368 nm.

resolution C 1s and N 1s spectra of CN, CN*, CPCN-1, and CPCN-1* are shown in Figure 2. The XPS C 1s spectra for all four samples consist of a major peak at 287.9 eV corresponding to the sp^2-hybridized C atoms in the form of heptazine (N−C═N), indicating that both doping and hydrothermal post-treatment did not change the fundamental framework of the graphitic carbon nitride network, in good agreement with the XRD and FT-IR results.[15] The peak at 284.5 eV was attributable to C atoms in the C═C or C−C.[6] The increased peak intensity at 284.5 eV for CPCN-1 and CPCN-1* compared to CN and CN*, respectively, indicated, once again, that C species were inserted into the resultant carbon nitride framework (Table S2). A new peak centered at 289.0 eV appeared in CN* and CPCN-1*, attributable to the formation of C−NH/NH_2 heptazine rings during the hydrothermal post-treatment.[45] The weak peak at 285.7 eV was assigned to C−O moieties due do the introduction of a trace amount of O during the polycondensation process under stable air atmosphere.[46] The XPS N 1s spectra (Figure 2b) were deconvoluted into 398.2, 399.5, 400.8, and 404.4 eV attributable to sp^2-hybridized N in C-containing heptazine rings (C−N═C), tertiary N in N-$(C)_3$ moieties, N in amino groups, and nitrate, respectively.[47,48] As shown in Figure 2c, the XPS P 2p spectrum of CPCN-1 can be deconvoluted into C−P and N−P bonds at 132.5 and 133.4 eV, respectively.[30,49] After the hydrothermal treatment, the N−P peak at 133.4 eV disappeared from the XPS P 2p spectrum of CPCN-1* shown in Figure 4d due to partial thermal decomposition of the N−P bonds. These results indicate the occurrence of C, P codoping of the carbon nitride framework, along with the slight P bleaching (*vide supra*).

The doping-induced modulation of electronic structures and properties could shift the optical adsorption of doped carbon nitride samples to longer wavelengths to allow for photocatalytic hydrogen generation under visible light. Compared to CN, CN*, and CPCN-1, CPCN-1* showed an adsorption tail over 450−650 nm (Figure 3a), indicating the importance of codoping to the band gap (E_g) modulation and hence possible visible light hydrogen generation. A simple comparison of CPCN-1* to CPCN-1 indicates that the value of E_g slightly increased after the hydrothermal treatment (Figure 3b,c), attributable to a small reduction of the effective conjugation length caused by the partial thermal decomposition with P leaching and/or the increasing ratio of substitutional C in CPCN-1*.[49]

Apart from a proper E_g, an energy level matching between the CB of a photocatalyst and the reduction potential of proton is also an important factor to determine whether or not the water splitting reaction could occur. By combining the Mott−Schottky plots (Figure S7) with the E_g values derived from Tauc plots (Figure 3b), we determined the energy levels of CB and VB for all the samples studied (Figure 3c).[26] From Figure S7, we could conclude that doping and hydrothermal post-treatment did not alter the semiconductor type of the samples as they all displayed the characteristic of an n-type semiconductor with a positive slope. From Figure 3c, it can be clearly seen that the CB energy levels of all the samples are below −0.39 eV (pH = 6.6 vs NHE), indicating that photoinduced electrons from all of these samples can overcome the thermodynamic barrier for reducing H^+ to H_2 under appropriate light irradiation.[10] As shown in Figure 3c, hydrothermal post-treatment of CN changed the energy level of CB, but barely VB. The improved CB level for CN* indicates it is a stronger reduction photocatalyst than CN. Although C and P codoping did not change the band gap (difference between CB and VB) of CN much, the energy levels of both CB and VB changed significantly (Figure 3c). The CB position of the CPCN-1 is 0.24 eV lower than that of CN, indicating that doping CN with C and P could significantly

DOI: 10.1021/acsami.7b02445
ACS Appl. Mater. Interfaces 2017, 9, 21730−21737

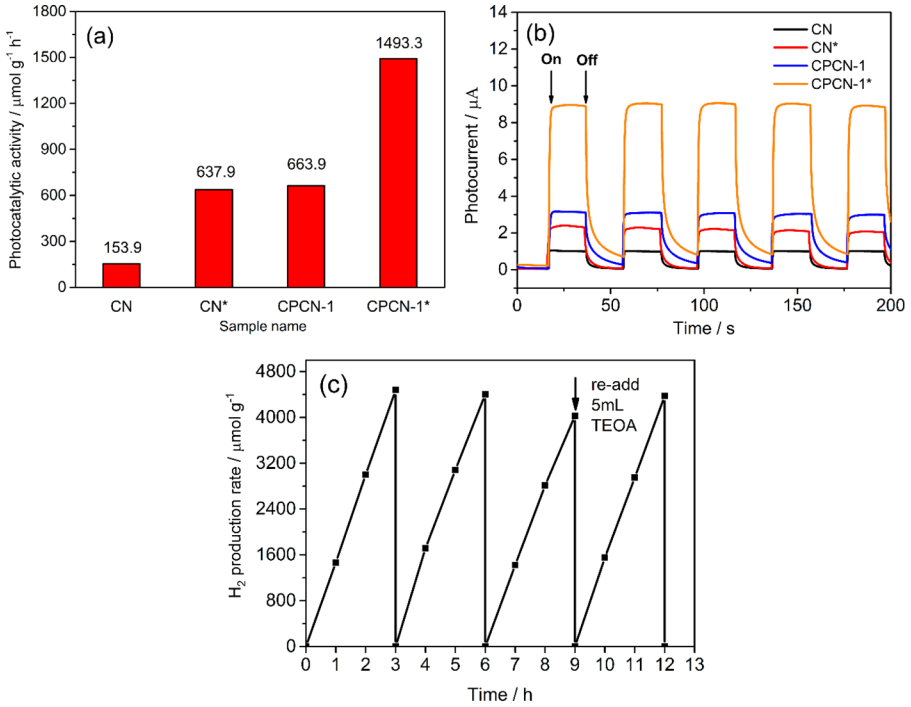

Figure 4. (a) Comparison of the photocatalytic activities for CN, CN*, CPCN-1, and CPCN-1* for the H_2 production using 20 vol % TEOA aqueous solution as a sacrificial reagent under visible-light irradiation (≥420 nm, 300 W Xe lamp). (b) Transient photocurrent responses of CN, CN*, CPCN-1, and CPCN-1* electrodes in 0.2 M Na_2SO_4 + 20 vol % TEOA mixed aqueous solution under visible-light irradiation. (c) Time course of photocatalytic H_2 production from CPCN-1*. The reaction system is purged with N_2 (200 sccm) every 3 h for 0.5 h to remove the H_2 inside.

enhance the photoreducibility of CN. For CPCN-1*, the energy level of CB fallen back to −1.303 eV because of partial P leaching during the hydrothermal post-treatment process, but it is still more negative than the corresponding value for CN*.[35] Compared to CN and CN*, therefore, CPCN-1* still has a stronger reducibility. Although CPCN-1 has a more negative CB and lower recombination of the photoinduced electron−hole pairs with respect to CPCN-1*, the CPCN-1* still has a higher H_2-generation rate (Figure 4a) because of its high specific surface area and large pore volume, good conductivity, and short transfer distance of carriers.

Photoluminescence (PL) was used to measure the efficiency of charge carrier trapping, transfer, and separation.[29] Figure 3d shows the PL emission spectra for CN, CN*, CPCN-1, and CPCN-1*. Doping CN with C and P can effectively inhabit the combination of generated charge carries, as evidenced by the dramatic reduce in intensity of the PL peak after doping. This is because C, P doping can effectively increase the transport properties of electrons. First, heteroatom dopants can behave as trapping sites to avoid the recombination of charge carries.[39] Second, increasing concentration of C element would improve the conductivity of samples (Figure S8). Last, the particle size were obviously reduced (Figure 3 and Figure S5). After hydrothermal treatment, the thermally induced partial structure decomposition could introduce more defects (e.g., −NH/NH_2 terminals, C−O species), and these defects could cause recombination of relatively more photogenerated electrons and holes with respect to CN, leading to more intense PL emission.[50] As can be also seen in Figure 3d, however, the PL emission intensity of CPCN-1* is still much lower than that of CN and CN*, indicating that CPCN-1* has excellent carrier transfer and separation capabilities attractive for photocatalysis.

Figures 4a and 4b show the photocatalytic activity and photocurrent responses over five on−off cycles in a three-electrode system, respectively. As expected, all the samples show a noticeable current increase upon visible light irradiation (λ > 420 nm), followed by a quick reverse back to the original state upon removal of the light source. The almost constant current intensity observed during different cycles under the light irradiation (Figure 4b) indicates a stable photocatalytic performance for all the samples tested. Among them, CPCN-1* exhibited the highest photocurrent response, which was almost ∼8 times higher than that of CN (Figure 4b). The observed dramatic enhancement in the photocurrent response for CPCN-1*, together with its relatively low PL intensity, confirmed that the combination of C- and P-doping and hydrothermal treatment has effectively improved the transfer capability and reduced the charge recombination.

We further investigated the photocatalytic performance of CN, CN*, CPCN-1, and CPCN-1* for hydrogen generation from the photocatalytic water splitting by using 1 wt % Pt as cocatalyst and 20 vol % TEOA as sacrificial reagent. Figure 4a,b shows a very low hydrogen generation rate (153.9 μmol g^{-1} h^{-1}) for CN due to its limited optical adsorption, small specific surface area, poor charge transport, and low photoinduced reducibility.[23] However, the low hydrogen generation rate of CN could be improved by doping and hydrothermal post-treatment. As can be seen in Figure S9, the H_2 generation rate of the CPCN-*X* increased with increasing the molar percentage of phytic acid in the starting materials to reach the highest rate for CPCN-1 and then decreased with further increasing in the C, P content. The H_2 generation rates of CN * and CPCN-1 are very close (637.6 μmol g^{-1} h^{-1} for CN* and 663.7 μmol g^{-1} h^{-1} for CPCN-1). For CN*, the improved photocatalytic performance with respect to CN is arising from the improved

DOI: 10.1021/acsami.7b02445
ACS Appl. Mater. Interfaces 2017, 9, 21730−21737

conductivity, increased SSA, and enhanced carrier mobility by the hydrothermal treatment (Figures 1 and 3, Figure S8). The specific surface area of CN* is about 3 times that of CN (Figure 1c), while the amount of H_2 generated by CN* is about 4 times that of CN (Figure 4a). Thus, increasing of C ratio would contribute to the observed improvement in the photocatalytic performance by improving conductivity. Compared to CN and CN*, CPCN-1 possesses an improved reductive capability of its photoinduced electrons (Figure 3c), enlarged adsorption range (Figures 3a,b), and reduced recombination rate of electron−hole pairs (Figure 3d) and hence a high photocatalytic performance (Figures 4a,b). Having the combined advantages of the C, P codoping and hydrothermal treatment, however, the CPCN-1* showed the highest H_2 generation rate of 1493.3 μmol g^{-1} h^{-1} (Figure 4a) because of high specific surface area and large pore volume, good conductivity, short transfer distance of carriers, and low recombination rate of carriers. From Figure 4 and specific parameters of the light source (λ = 420 nm filter, 300 W Xe lamp) that we used, eq S2 gave an AQE of 2.14% for CPCN-1*, which was compared with that of other g-C_3N_4 based photocatalysts in Table S2 (detailed calculation is shown in the Supporting Information). We noticed that the value of 2.14% for the CPCN-1* under 420 nm visible light is among the high end of the corresponding values for all the −C_3N_4-based photocatalysts.

Figure 4c demonstrates the typical stability of CPCN-1* over four cycles (more cycles are listed in Figure S11), which shows that the H_2 generation rate of CPCN-1* slowly decreased during the initial three cycles due to the continued consumption of TEOA in the photocatalytic system. As expected, the H_2-generation rate recovered to the initial value (1493.3 μmol g^{-1} h^{-1}) upon the addition of 5 mL of TEOA into the system once the third cycle was completed. Figure S12 shows the XRD, SEM, TEM, and deconvoluted XPS data after the stability test, and no obvious change was observed for CPCN-1*. Therefore, CPCN-1* possesses a good stability, and the observed excellent photocatalytic activity and stability could be attributed to its large specific surface area, fast carrier transfer, and efficient visible light adsorption resulted from the synergistic effect of codoping and hydrothermal treatment. More specifically, the C, P codoping decreased CB to −1.303 eV (more negative than that of CN, −1.163 eV) for an increased reduceability, reduced the recombination of photoinduced carriers, and enhanced conductivity, while the hydrothermal treatment increased the specific surface area and volume ratio of mesopores to facilitate the mass transfer process and hence the overall photocatalytic H_2 generation on the CPCN-1*.

4. CONCLUSION

In summary, we have successfully prepared a C, P-codoped g-C_3N_4 by assembling melamine with phytic acid into C, P-doped g-C_3N_4, followed by hydrothermal treatment to increase the composition ratio of C. During the hydrothermal treatment, the specific surface area and pore volume of C, P-doped g-C_3N_4 were significantly increased and the concentration change of C and P in the lattice of g-C_3N_4 further modulated bandgap, reduced the hole-electron recombination, and increased conductivity, leading to enhanced photocatalytic properties for hydrogen generation by photocatalytic water splitting. Under visible light irradiation ($\lambda \geq 420$ nm), the resultant C, P-codoped g-C_3N_4 (i.e., CPCN-1) after the hydrothermal treatment (i.e., CPCN-1*) showed a H_2 generation rate up to 1493.3 μmol g^{-1} h^{-1}, which is 9.7 times higher than that of the bulk pristine g-C_3N_4. The apparent quantum efficiency (AQE) of CPCN-1* was calculated to be 2.14% under the visible light, which was relative high among of all reported carbon-based metal-free photocatalysts ever at 420 nm.

■ ASSOCIATED CONTENT

Supporting Information

The Supporting Information is available free of charge on the ACS Publications website at DOI: 10.1021/acsami.7b02445.

Calculation details of H_2-generation rate and AQE, stability test condiation of 20-cycle, XRD pattern and H_2-generation rate of CPCN-X, FT-IR, XPS, Mott−Schottky plot, typical SEM and TEM images of CN, CN*, CPCN-1, and CPCN-1*, EIS of CN, CN*, CPCN-1, and CPCN-1*, HRTEM of CN and CPCN-1, EDS mapping data of CPCN-1, and XRD, SEM, TEM, and deconvoluted XPS spectra of CPCN-1* after stability test (PDF)

■ AUTHOR INFORMATION

Corresponding Author

*E-mail: liming.dai@case.edu.

ORCID

Liming Dai: 0000-0001-7536-160X

Notes

The authors declare no competing financial interest.

■ ACKNOWLEDGMENTS

The authors thank the financial support from NSFC, The 111 Project (B14004), State Key Laboratory of Organic−Inorganic Composites, Beijing Municipal Science & Technology Commission, Beijing Advanced Innovation Center for Soft Matter Science and Engineering, BUCT, and CWRU.

■ REFERENCES

(1) Fujishima, A.; Honda, K. Electrochemical Photolysis of Water at a Semiconductor Electrode. *Nature* **1972**, *238* (238), 37−38.

(2) Ong, W.; Tan, L.; Ng, Y.; Yong, S.; Chai, S. Graphitic Carbon Nitride g-C_3N_4-Based Photocatalysts for Artificial Photosynthesis and Environmental Remediation: Are We a Step Closer To Achieving Sustainability? *Chem. Rev.* **2016**, *116* (12), 7159−7329.

(3) Zhang, G.; Lan, Z.-A.; Wang, X. Conjugated Polymers: Catalysts for Photocatalytic Hydrogen Evolution. *Angew. Chem., Int. Ed.* **2016**, *55*, 15712−15727.

(4) Liu, J.; Liu, Y.; Liu, N.; Han, Y.; Zhang, X.; Huang, H.; Lifshitz, Y.; Lee, S.-T.; Zhong, J.; Kang, Z. Metal-free Efficient Photocatalyst for Stable Visible Water Splitting via a Two-electron Pathway. *Science* **2015**, *347* (6225), 970−974.

(5) Wang, X.; Carlsson, J. M.; Domen, K.; Antonietti, M.; Maeda, K.; Thomas, A.; Takanabe, K. A Metal-free Polymeric Photocatalyst for Hydrogen Production from Water Under Visible Light. *Nat. Mater.* **2009**, *8* (1), 76−80.

(6) Yu, H.; Shang, L.; Bian, T.; Shi, R.; Waterhouse, G. I. N.; Zhao, Y.; Zhou, C.; Wu, L.-Z.; Tung, C.-H.; Zhang, T. Nitrogen-Doped Porous Carbon Nanosheets Templated from g-C_3N_4 as Metal-Free Electrocatalysts for Efficient Oxygen Reduction Reaction. *Adv. Mater.* **2016**, *28* (25), 5080−5086.

(7) Li, K.; Yan, L.; Zeng, Z.; Luo, S.; Luo, X.; Liu, X.; Guo, H.; Guo, Y. Fabrication of $H_3PW_{12}O_{40}$-doped Carbon Nitride Nanotubes by One-step Hydrothermal Treatment Strategy and Their Efficient Visible-light Photocatalytic Activity toward Representative Aqueous persistent Organic Pollutants Degradation. *Appl. Catal., B* **2014**, *156−157*, 141−152.

DOI: 10.1021/acsami.7b02445
ACS Appl. Mater. Interfaces 2017, 9, 21730−21737

(8) Liu, J.; Xie, S.; Geng, Z.; Huang, K.; Fan, L.; Zhou, W.; Qiu, L.; Gao, D.; Ji, L.; Duan, L.; Lu, L.; Li, W.; Bai, S.; Liu, Z.; Chen, W.; Feng, S.; Zhang, Y. Carbon Nitride Supramolecular Hybrid Material Enabled High-Efficiency Photocatalytic Water Treatments. *Nano Lett.* **2016**, *16* (10), 6568−6575.
(9) Duan, J.; Chen, S.; Jaroniec, M.; Qiao, S. Z. Porous C_3N_4 Nanolayers@N-Graphene Films as Catalyst Electrodes for Highly Efficient Hydrogen Evolution. *ACS Nano* **2015**, *9* (1), 931−940.
(10) Shinde, S. S.; Sami, A.; Lee, J.-H. Sulfur Mediated Graphitic Carbon Nitride/S-Se-graphene as a Metal-free Hybrid Photocatalyst for Pollutant Degradation and Water Splitting. *Carbon* **2016**, *96*, 929−936.
(11) Shinde, S. S.; Lee, C. H.; Sami, A.; Kim, D. H.; Lee, S. U.; Lee, J. H. Scalable 3-D Carbon Nitride Sponge as an Efficient Metal-Free Bifunctional Oxygen Electrocatalyst for Rechargeable Zn-Air Batteries. *ACS Nano* **2017**, *11* (1), 347−357.
(12) Xu, J.; Li, Y.; Peng, S. Photocatalytic Hydrogen Evolution over Erythrosin B-sensitized Graphitic Carbon Nitride with In situ Grown Molybdenum Sulfide Cocatalyst. *Int. J. Hydrogen Energy* **2015**, *40* (1), 353−362.
(13) Xu, J.; Li, Y.; Peng, S.; Lu, G.; Li, S. Eosin Y-sensitized Graphitic Carbon Nitride Fabricated by Heating Urea for Visible Light Photocatalytic Hydrogen Evolution: the Effect of the Pyrolysis Temperature of Urea. *Phys. Chem. Chem. Phys.* **2013**, *15* (20), 7657−7665.
(14) Guo, F.; Chen, J.; Zhang, M.; Gao, B.; Lin, B.; Chen, Y. Deprotonation of g-C_3N_4 with Na Ions for Efficient Nonsacrificial Water Splitting under Visible Light. *J. Mater. Chem. A* **2016**, *4* (28), 10806−10809.
(15) Li, H.-J.; Qian, D.-J.; Chen, M. Templateless Infrared Heating Process for Fabricating Carbon Nitride Nanorods with Efficient Photocatalytic H_2 Evolution. *ACS Appl. Mater. Interfaces* **2015**, *7* (45), 25162−25170.
(16) Ishida, Y.; Chabanne, L.; Antonietti, M.; Shalom, M. Morphology Control and Photocatalysis Enhancement by the One-pot Synthesis of Carbon Nitride from Preorganized Hydrogen-bonded Supramolecular Precursors. *Langmuir* **2014**, *30* (2), 447−451.
(17) Xu, J.; Wang, Y.; Zhu, Y. Nanoporous Graphitic Carbon Nitride with Enhanced Photocatalytic Performance. *Langmuir* **2013**, *29* (33), 10566−10572.
(18) Jun, Y. S.; Lee, E. Z.; Wang, X.; Hong, W. H.; Stucky, G. D.; Thomas, A. From Melamine-Cyanuric Acid Supramolecular Aggregates to Carbon Nitride Hollow Spheres. *Adv. Funct. Mater.* **2013**, *23* (29), 3661−3667.
(19) Su, J.; Zhu, L.; Geng, P.; Chen, G. Self-assembly Graphitic Carbon Nitride Quantum Dots Anchored on TiO_2 Nanotube Arrays: An Efficient Heterojunction for Pollutants Degradation under Solar Light. *J. Hazard. Mater.* **2016**, *316*, 159−168.
(20) Qin, Y.; Li, J.; Yuan, J.; Kong, Y.; Tao, Y.; Lin, F.; Li, S. Hollow Mesoporous Carbon Nitride Nanosphere/Three-dimensional Graphene Composite as High Efficient Electrocatalyst for Oxygen Reduction Reaction. *J. Power Sources* **2014**, *272*, 696−702.
(21) Ma, T. Y.; Cao, J. L.; Jaroniec, M.; Qiao, S. Interacting Carbon Nitride and Titanium Carbide Nanosheets for High-Performance Oxygen Evolution. *Angew. Chem., Int. Ed.* **2016**, *55* (3), 1138−1142.
(22) Chen, X.; Zhang, J.; Fu, X.; Antonietti, M.; Wang, a. X. Fe-g-C_3N_4-Catalyzed Oxidation of Benzene to Phenol Using Hydrogen Peroxide and Visible Light. *J. Am. Chem. Soc.* **2009**, *131*, 11658−11659.
(23) Gao, L.-F.; Wen, T.; Xu, J.-Y.; Zhai, X.-P.; Zhao, M.; Hu, G.-W.; Chen, P.; Wang, Q.; Zhang, H.-L. Iron-Doped Carbon Nitride-Type Polymers as Homogeneous Organocatalysts for Visible Light-Driven Hydrogen Evolution. *ACS Appl. Mater. Interfaces* **2016**, *8* (1), 617−624.
(24) Hu, S.; Ma, L.; You, J.; Li, F.; Fan, Z.; Lu, G.; Liu, D.; Gui, J. Enhanced Visible Light Photocatalytic Performance of g-C_3N_4 Photocatalysts Co-doped with Iron and Phosphorus. *Appl. Surf. Sci.* **2014**, *311*, 164−171.
(25) Xu, C.; Han, Q.; Zhao, Y.; Wang, L.; Li, Y.; Qu, L. Sulfur-doped Graphitic Carbon Nitride Decorated with Graphene Quantum Dots for an Efficient Metal-free Electrocatalyst. *J. Mater. Chem. A* **2015**, *3* (5), 1841−1846.
(26) Ran, J.; Ma, T. Y.; Gao, G.; Du, X.-W.; Qiao, S. Z. Porous P-doped Graphitic Carbon Nitride Nanosheets for Synergistically Enhanced Visible-light Photocatalytic H_2 Production. *Energy Environ. Sci.* **2015**, *8* (12), 3708−3717.
(27) Cao, S.; Low, J.; Yu, J.; Jaroniec, M. Polymeric Photocatalysts Based on Graphitic Carbon Nitride. *Adv. Mater.* **2015**, *27* (13), 2150−2176.
(28) Patnaik, S.; Martha, S.; Madras, G.; Parida, K. The Effect of Sulfate Pre-treatment to Improve the Deposition of Au-Nanoparticles in a Gold-modified Sulfated g-C_3N_4 Plasmonic Photocatalyst towards Visible Light Induced Water Reduction Reaction. *Phys. Chem. Chem. Phys.* **2016**, *18* (41), 28502−28514.
(29) Wang, Y.; Zhang, J.; Wang, X.; Antonietti, M.; Li, H. Boron- and Fiuorine-containing Mesoporous Carbon Nitride Polymers: Metal-free Catalysts for Cyclohexane Oxidation. *Angew. Chem., Int. Ed.* **2010**, *49* (19), 3356−3359.
(30) Zhou, Y.; Zhang, L.; Liu, J.; Fan, X.; Wang, B.; Wang, M.; Ren, W.; Wang, J.; Li, M.; Shi, J. Brand new P-doped g-C_3N_4: Enhanced Photocatalytic Activity for H_2 Evolution and Rhodamine B Degradation under Visible Light. *J. Mater. Chem. A* **2015**, *3* (7), 3862−3867.
(31) Bhunia, M. K.; Melissen, S.; Parida, M. R.; Sarawade, P.; Basset, J.-M.; Anjum, D. H.; Mohammed, O. F.; Sautet, P.; Le Bahers, T.; Takanabe, K. Dendritic Tip-on Polytriazine-Based Carbon Nitride Photocatalyst with High Hydrogen Evolution Activity. *Chem. Mater.* **2015**, *27* (24), 8237−8247.
(32) Chen, W.; Liu, T.-Y.; Huang, T.; Liu, X.-H.; Yang, X.-J. Novel Mesoporous P-doped Graphitic Carbon Nitride Nanosheets Coupled with $ZnIn_2S_4$ Nanosheets as Efficient Visible Light Driven Heterostructures with Remarkably Enhanced Photo-reduction Activity. *Nanoscale* **2016**, *8* (6), 3711−3719.
(33) Jun, Y.-S.; Lee, E. Z.; Wang, X.; Hong, W. H.; Stucky, G. D.; Thomas, A. From Melamine-Cyanuric Acid Supramolecular Aggregates to Carbon Nitride Hollow Spheres. *Adv. Funct. Mater.* **2013**, *23* (29), 3661−3667.
(34) Fan, H.; Wang, N.; Tian, Y.; Ai, S.; Zhan, J. Acetic Acid Induced Synthesis of Laminated Activated Carbon Nitride Nanostructures. *Carbon* **2016**, *107*, 747−753.
(35) Han, Q.; Wang, B.; Gao, J.; Cheng, Z.; Zhao, Y.; Zhang, Z.; Qu, L. Atomically Thin Mesoporous Nanomesh of Graphitic C_3N_4 for High-Efficiency Photocatalytic Hydrogen Evolution. *ACS Nano* **2016**, *10* (2), 2745−2751.
(36) Wang, X.-J.; Tian, X.; Li, F.-t.; Li, Y.-p.; Zhao, J.; Hao, Y.-J.; Liu, Y. Synchronous Surface Hydroxylation and Porous Modification of g-C_3N_4 for Enhanced Photocatalytic H_2 Evolution Efficiency. *Int. J. Hydrogen Energy* **2016**, *41* (6), 3888−3895.
(37) Yang, S.; Gong, Y.; Zhang, J.; Zhan, L.; Ma, L.; Fang, Z.; Vajtai, R.; Wang, X.; Ajayan, P. M. Exfoliated Graphitic Carbon Nitride Nanosheets as Efficient Catalysts for Hydrogen Evolution under Visible Light. *Adv. Mater.* **2013**, *25* (17), 2452−2456.
(38) Zhang, J.; Qu, L.; Shi, G.; Liu, J.; Chen, J.; Dai, L. N,P-Codoped Carbon Networks as Efficient Metal-free Bifunctional Catalysts for Oxygen Reduction and Hydrogen Evolution Reactions. *Angew. Chem., Int. Ed.* **2016**, *55* (6), 2230−2234.
(39) Dong, G.; Zhao, K.; Zhang, L. Carbon Self-doping Induced High Electronic Conductivity and Photoreactivity of g-C_3N_4. *Chem. Commun. (Cambridge, U. K.)* **2012**, *48* (49), 6178−6180.
(40) Fina, F.; Callear, S. K.; Carins, G. M.; Irvine, J. T. S. Structural Investigation of Graphitic Carbon Nitride via XRD and Neutron Diffraction. *Chem. Mater.* **2015**, *27* (7), 2612−2618.
(41) Liu, S.; Sun, H.; O'Donnell, K.; Ang, H. M.; Tade, M. O.; Wang, S. Metal-free Melem/g-C_3N_4 Hybrid Photocatalysts for Water Treatment. *J. Colloid Interface Sci.* **2016**, *464*, 10−17.
(42) Sano, T.; Tsutsui, S.; Koike, K.; Hirakawa, T.; Teramoto, Y.; Negishi, N.; Takeuchi, K. Activation of Graphitic Carbon Nitride (g-

DOI: 10.1021/acsami.7b02445
ACS Appl. Mater. Interfaces 2017, 9, 21730−21737

C3N4) by Alkaline Hydrothermal Treatment for Photocatalytic NO Oxidation in Gas Phase. *J. Mater. Chem. A* **2013**, *1* (21), 6489.
(43) Konda, S. K.; Amiri, M.; Chen, A. Photoassisted Deposition of Palladium Nanoparticles on Carbon Nitride for Efficient Oxygen Reduction. *J. Phys. Chem. C* **2016**, *120* (27), 14467−14473.
(44) Li, Y.; Zhang, J.; Wang, Q.; Jin, Y.; Huang, D.; Cui, Q.; Zou, G. Nitrogen-Rich Carbon Nitride Hollow Vessels: Synthesis, Characterization, and Their Properties. *J. Phys. Chem. B* **2010**, *114*, 9429−9434.
(45) Li, X.; Hartley, G.; Ward, A. J.; Young, P. A.; Masters, A. F.; Maschmeyer, T. Hydrogenated Defects in Graphitic Carbon Nitride Nanosheets for Improved Photocatalytic Hydrogen Evolution. *J. Phys. Chem. C* **2015**, *119* (27), 14938−14946.
(46) Li, Y.; Xu, H.; Ouyang, S.; Lu, D.; Wang, X.; Wang, D.; Ye, J. In situ Surface Alkalinized g-C_3N_4 toward Enhancement of Photocatalytic H_2 Evolution under Visible-light Irradiation. *J. Mater. Chem. A* **2016**, *4* (8), 2943−2950.
(47) Ma, T. Y.; Ran, J.; Dai, S.; Jaroniec, M.; Qiao, S. Z. Phosphorus-doped Graphitic Carbon Nitrides Grown In situ on Carbon-fiber Paper: Flexible and Reversible Oxygen Electrodes. *Angew. Chem., Int. Ed.* **2015**, *54* (15), 4646−4650.
(48) Lin, L.; Ou, H.; Zhang, Y.; Wang, X. Tri-s-triazine-Based Crystalline Graphitic Carbon Nitrides for Highly Efficient Hydrogen Evolution Photocatalysis. *ACS Catal.* **2016**, *6* (6), 3921−3931.
(49) Guo, S.; Deng, Z.; Li, M.; Jiang, B.; Tian, C.; Pan, Q.; Fu, H. Phosphorus-Doped Carbon Nitride Tubes with a Layered Micro-nanostructure for Enhanced Visible-Light Photocatalytic Hydrogen Evolution. *Angew. Chem., Int. Ed.* **2016**, *55* (5), 1830−1834.
(50) Hu, S.; Ma, L.; Xie, Y.; Li, F.; Fan, Z.; Wang, F.; Wang, Q.; Wang, Y.; Kang, X.; Wu, G. Hydrothermal Synthesis of Oxygen Functionalized S-P Codoped g-C_3N_4 Nanorods with Outstanding Visible Light Activity under Anoxic Conditions. *Dalton Trans.* **2015**, *44* (48), 20889−20897.

DOI: 10.1021/acsami.7b02445
ACS Appl. Mater. Interfaces 2017, 9, 21730−21737